Annals of Nuclear Energy 200 (2024) 110408

Contents lists available at ScienceDirect

Annals of Nuclear Energy

journal homepage: www.elsevier.com/locate/anucene

Manufacturing high-uranium-loaded dispersion fuel plates in Brazil

Michelangelo Durazzo [a,*], Jose Antonio Batista Souza [a], Elita Fontenele Urano de Carvalho [a], Thomaz Augusto Guisard Restivo [b], Frederico Antonio Genezini [a], Ricardo Mendes Leal Neto [a]

[a] Nuclear and Energy Research Institute, IPEN-CNEN/SP, São Paulo, SP, Brazil
[b] University of Sorocaba, UNISO, Sorocaba, SP, Brazil

ARTICLE INFO

Keywords:
Fuel plate
Fuel element
Uranium silicide
Dispersions
Research reactor
Nuclear fuel
Fabrication

ABSTRACT

The Nuclear and Energy Research Institute (IPEN-CNEN/SP) has developed and made available for routine production the technology for manufacturing dispersion-type fuel elements for research reactors. However, the fuel produced is limited to a uranium loading of 2.3 gU/cm^3 (U_3O_8) or 3.0 gU/cm^3 (U_3Si_2). To reduce Brazil's dependence on foreign sources of Mo-99, the Brazilian government plans to construct a new research reactor, the 30 MW open pool Brazilian Multipurpose Reactor (RMB), which will mainly produce domestic Mo-99. Low-enriched uranium fuel will be used in the RMB, and increasing uranium loading will be important to increase the reactor core's reactivity and fuel life. Uranium loadings of 3.2 gU/cm^3 for the U_3O_8-Al and 4.8 gU/cm^3 for the U_3Si_2-Al are considered the technological limit and have been well demonstrated worldwide. This work aimed to study the manufacturing process of these two highly uranium-loaded dispersion fuels and redefine current procedures. Additionally, UMo-Al dispersion fuel has been extensively studied globally and is likely to be the next commercially available technology. This new fuel utilizes a dispersion of UMo alloy with 7–10 wt% Mo, resulting in a uranium loading between 6 and 8 gU/cm^3. We also studied this fuel type for potential use in the RMB research reactor. This work outlines the primary procedures for manufacturing these three types of fuels and the necessary adjustments to IPEN-CNEN/SP current technology. The manufacturing process proved to be well adapted to these new fuels, requiring only minor modifications. A comparison was made of the microstructures of fuel plate meat using three types of uranium compounds. The microstructures of U_3Si_2-Al and U10Mo-Al dispersions were found to be adequate, while that of U_3O_8-Al meat deviated significantly from the concept of an ideal dispersion.

1. Introduction

Brazil presently operates four research reactors, the most important of which is the pool-type 5 MW IEA-R1. The other three are the 100 W critical facility IPEN/MB-01, the 500 W ARGONAUTA (Argonaut type), and the 100 kW TRIGA type IPR-R1. IPEN routinely produces the plate-type fuel required for these research reactors, except for IPR-R1.

Brazil's need for Mo-99, a critical element used in nuclear medicine, has been met through imports due to its unavailability at IEA-R1, Brazil's most powerful research reactor. However, global shortages of Mo-99 in 2009–2010 and 2017–2018 (Nuclear Energy Agency, 2019) have affected Brazil, prompting the government to construct a new research reactor specifically designed for domestic Mo-99 production (Obadia and Perrotta, 2010). The new pool-type reactor will operate using low-enriched uranium (LEU) fuel, generating 30 MW of power, and will be located roughly 100 km from São Paulo, in southeast Brazil, as part of a new nuclear research center. The Brazilian Multipurpose Reactor (RMB) project, as it is called, has been discussed in detail by Perrotta and Soares (2014), and the new research center will include various facilities, as described by Perrotta and Obadia (2011). The objective of this initiative is to produce fuel in Brazil to support the operation of the RMB research reactor.

Since the end of the 1980s, the Nuclear and Energy Research Institute (IPEN-CNEN/SP) has produced 1151 fuel plates based on the U_3O_8-Al dispersion. Of these, 450 with uranium loading of 1.9 gU/cm^3 (25 fuel elements), and 666 with uranium loading of 2.3 gU/cm^3 (37 fuel elements). The IEA-R1 research reactor consumed 1116 of these fuel plates, and the Argonaut reactor consumed 35.

The production of fuel plates based on U_3Si_2-Al dispersion by IPEN-CNEN/SP started in 2007, and since then, 990 plates with uranium

* Corresponding author at: Av. Prof. Lineu Prestes, 2242, Cidade Universitária, CEP 05508-000 São Paulo, SP, Brazil.
E-mail addresses: mdurazzo@ipen.br (M. Durazzo), jasouza@ipen.br (J.A.B. Souza), elitaucf@ipen.br (E.F. Urano de Carvalho), thomaz@protolab.com.br (T.A.G. Restivo), fredzini@ipen.br (F.A. Genezini), lealneto@ipen.br (R.M. Leal Neto).

https://doi.org/10.1016/j.anucene.2024.110408
Received 9 May 2023; Received in revised form 28 December 2023; Accepted 2 February 2024
Available online 6 February 2024

loading of 3.0 gU/cm^3 for IEA-R1 research reactor (consisting of 55 fuel elements) have been manufactured. In 2018, IPEN-CNEN/SP produced 399 fuel plates, each with 3.0 gU/cm^3, to form the core of the IPEN-MB-01 research reactor, which consists of 19 fuel elements. The specifications of these fuel plates are identical to those intended for use in the RMB.

Fuel elements containing both types of fuel plates, U_3O_8-Al and U_3Si_2-Al, have been successfully used in the IEA-R1 reactor. These fuel elements have achieved a burn-up of about 50 % for both fuel types after seven years of irradiation, without encountering any issues.

The fuel elements manufactured at IPEN-CNEN/SP are of the MTR (Materials Testing Reactor) type (Cunningham and Boyle, 1955). They are built by assembling a number of fuel plates with sufficient spacing between them to allow the flow of water, which serves as both coolant and moderator. The fuel plates are formed by a containing fissile material meat, which is entirely protected with an aluminum cladding (Weber and Hirsch, 1955). The fuel plates are manufactured using a traditional method, known internationally as the "picture frame technique", shown in Fig. 1 (Durazzo and Riella, 2015; Kaufman, 1962). This involves inserting the fuel meat (also called "briquette") into an aluminum frame and covering it with aluminum plates that are then rolled together.

"Briquettes," or fuel meats, are produced employing powder metallurgy methods. The nuclear fuel material for the fuel meats is U_3O_8 or U_3Si_2 powder which is enriched with 20 wt% in the U-235 isotope, while aluminum powder is the structural material for the meat matrix.

As shown in Fig. 2, the MTR-type fuel is composed of an array of parallel fuel plates that are rigidly put together to form the fuel element.

Maintaining a continuous aluminum matrix within the fuel meat is fundamental to the dispersion fuel concept. Due to this requirement, the technological limit for dispersions is 45 vol% of fissile material dispersed. IPEN-CNEN/SP has historically employed volume fractions of 33 % (U_3O_8) and 27 % (U_3Si_2), corresponding to respective uranium loadings of 2.3 and 3.0 gU/cm^3. As a result, the current fuel may still contain a significant amount of added uranium.

This work presents the results of developing the manufacturing process for fuel plates with high uranium loadings using 45 vol% of the dispersed phase in the U_3O_8-Al and U_3Si_2-Al dispersions. The necessary adjustments to the currently adopted procedures are described.

Uranium loading close to 7 gU/cm^3 can be achieved using the U10Mo alloy (10 wt% Mo). The viability of the use of this type of fuel in the IEA-R1 research reactor has been studied (Silva et al., 2008), and its use in the RMB research reactor has also been proposed. Fabrication of miniplates of U10Mo-Al dispersion with 45 vol% was investigated before (Durazzo et al., 2014). The manufacturing of full-size plates of this fuel needs to be checked. The results are presented and discussed.

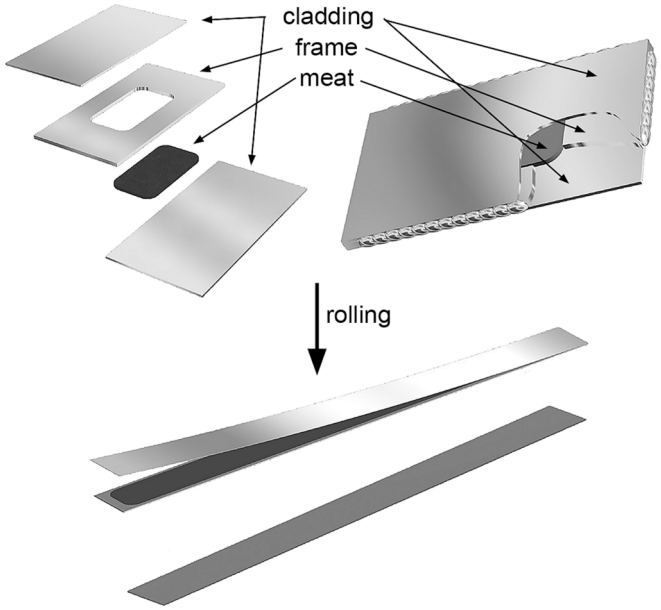

Fig. 1. Picture frame technique used to manufacture fuel plates.

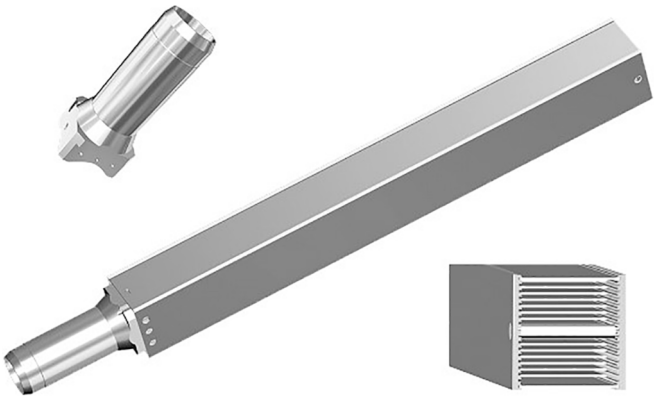

Fig. 2. Fuel element for the IEA-R1 research reactor.

2. Material and methods

In research reactors, the fuel of the dispersion plate type is most frequently used. Most manufacturing procedures apply to fuel plates manufactured from any dispersion type, except for the powder preparation step. Although the manufacturing and inspection procedures are similar for the various manufacturers of fuel plates, the procedures used in this work are specific to the case of IPEN-CNEN/SP. There is little literature available that describes the manufacturing process of dispersion fuel plates. The published information is outdated, not detailed, and specific to the fuel of a given research reactor (Kucera et al., 1963; Beaver et al., 1964; Knight et al., 1968; Knight and Morin, 1999).

The initial stages of manufacturing mainly involve chemical processes. The manufacturing process starts with low-enriched uranium hexafluoride (UF_6). When UF_6 is injected into the water, it immediately hydrolyzes, reacting with water to form a uranyl fluoride (UO_2F_2) solution. After this step, the procedure was divided into two routes: one for producing U_3O_8 powder and the other for producing U_3Si_2 and U10Mo powders. In this work, natural uranium was used.

2.1. U_3O_8 powder fabrication

The U_3O_8 powder was obtained from ammonium diuranate (ADU), precipitated with ammonia from the solution of uranyl fluoride. The ADU powder was calcined at 600 °C for 3 h to transform into U_3O_8 completely. The calcination was performed in the air using Inconel boats in a resistive furnace.

The calcined U_3O_8 powder was granulated by pressing and subsequently crushing the pellets. The pressing was carried out in a hydraulic press with a 40 mm diameter floating-type cylindrical die at a pressure of 156 MPa. The pellets (weighting 50 g) were manually ground in a mortar. The U_3O_8 powder was then sieved to obtain granules within the 150–44 μm size range. The granules were sintered at 1400 °C for 6 h. The material was classified again, and the 125–44 μm fraction was separated. A maximum of 20 wt% of the fraction less than 44 μm was used. The powder's density of 8.35 g/cm^3 was measured using a helium pycnometer. Fig. 3 presents the typical morphology of the U_3O_8 powder.

2.2. U_3Si_2 powder fabrication

The route to prepare both the U_3Si_2 and U10Mo powders was through UF_4 and uranium metal. $SnCl_2$ was used as a reducing agent

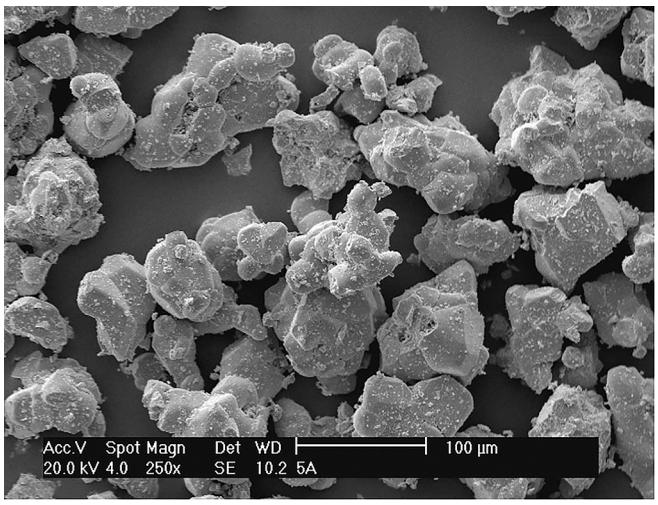

Fig. 3. SEM micrograph (secondary electrons image) of U_3O_8 powder particles.

during the reduction/precipitation process to produce UF_4 from the uranyl fluoride solution. The precipitated UF_4 in suspension was transferred to a filtration system from the precipitation reactor. The material in the filter was collected and dried to remove free water. The UF_4 was then heated in argon to remove the water from crystallization. The UF_4 was ready to produce uranium metal after the second drying procedure.

It is simpler to produce uranium metal via the magnesiothermic reduction of UF_4 and avoids dealing with poisonous and pyrophoric calcium. A graphite crucible was filled with a reagent charge that included 1540 g of UF_4 and 270 g of Mg (15 % extra Mg over the stoichiometric quantity).

The charge was prepared to maintain the homogeneity of the Mg and UF_4 mixture. Because of the materials' significantly different densities ($\rho_{Mg} = 1.74$ g/cm^3 and $\rho_{UF4} = 6.72$ g/cm^3), a stratified charge was made. The charge of UF_4 + Mg was divided into ten layers and tapped one by one into the graphite crucible for homogenization. The crucible was fabricated of fully machined graphite volume with sufficient resistance to generate about 1000 g of uranium metal. A variable amount of CaF_2 was tapped over the UF_4 + Mg charge to complete the crucible reaction volume. The crucible was closed with the graphite top cover and mounted within an ANSI 310 stainless steel cylindrical reactor vessel, which permits argon fluxing during batch processing (1 L/min with 0.2 MPa of pressure).

A resistor pit furnace with four programmable zones that could raise the temperature to 1200 °C accommodates the whole crucible and reactor. The reactants spontaneously ignited when the reaction vessel was heated. The procedure produces liquid MgF_2 slag and uranium metal. After opening the crucible, both products descended to the bottom and were quickly separated. Ten minutes were given after the reaction to allow the reaction products to solidify completely inside the furnace. The reactor vessel was then lifted out of the furnace after the furnace had been switched off. Fig. 4 shows the uranium metal ingot.

To recover uranium from the MgF_2 slag, it was first calcinated in the air to promote oxidation to U_3O_8. The uranium present in the slag was then extracted by leaching with HNO_3. The resulting uranyl nitrate solution ($UO_2(NO_3)_2$) was impure and required further purification. The purified uranium was then reintroduced into the process via ADU precipitation. Details on uranium metal production at IPEN-CNEN/SP are available in previous work (Durazzo et al., 2017a). Uranium metal is not only used in the fuel production but also in the manufacture of irradiation targets to produce Mo-99 (Durazzo et al., 2021; Durazzo et al., 2022).

The intermetallic U_3Si_2 was produced using an induction furnace from uranium metal (92.5 wt%) and metallic silicon (7.5 wt%), molten inside a zirconia crucible specially designed to reach temperatures above 1750 °C. The induction furnace was placed under a vacuum of 0.13 Pa and flushed with an argon atmosphere.

Fig. 4. Uranium metal ingot.

The U_3Si_2 ingot was handled inside a glove box with an inert argon atmosphere. After crushing the ingot, granules less than 4 mm in size were obtained and then sieved. The sieve set consisted of a backdrop compartment, a fine sieve with a 125 µm opening, and a coarse sieve with a 4 mm opening. Granules with a diameter greater than 4 mm were crushed again, while granules with sizes between 4 mm and 125 µm were collected for final grinding. The final grinding was carried out carefully to separate the powder from 125 to 44 µm with intermediate sieving. The use of particles smaller than 44 µm was restricted to a maximum of 20 %. The powder's density of 12.00 g/cm^3 was determined using a helium pycnometer. Fig. 5 shows the typical U_3Si_2 powder morphology. According to the X-ray diffractogram shown in Fig. 6, only U_3Si_2 phase was present.

2.3. U10Mo powder fabrication

The process of producing U-Mo powder has been studied at the IPEN-CNEN/SP since 2014 using the hydriding-milling-dehydriding (HMD) route (Leal Neto et al., 2014; Durazzo et al., 2014). Induction melting was used to melt U-Mo alloy ingots with a 10 wt% Mo concentration in a zirconia crucible. The raw materials used were molybdenum and uranium metals with 99.95 % purity. Both materials were charged into the zirconia crucible and inducted up to melting in a high-purity argon environment. The outcome was an ingot that was nearly 40 mm in diameter and 50 mm in height, and weighed about 1200 g. The ingot was then subjected to a 72-hour treatment at 1000 °C in a reactor filled with pure argon before being rapidly cooled to preserve the gamma

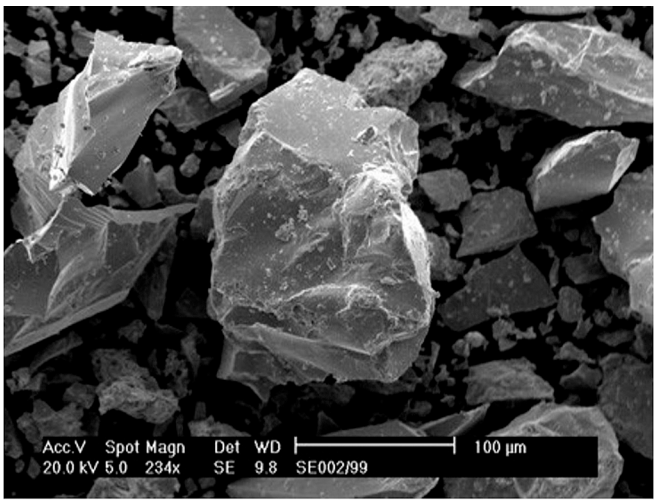

Fig. 5. SEM micrograph (secondary electrons image) of the U_3Si_2 powder particles.

phase. It was next divided into pieces for powder preparation by hydriding-milling-dehydriding (HMD). Further details on U10Mo powder preparation process can be found in previous work (Leal Neto et al., 2014; Durazzo et al., 2014).

Five pieces were taken from the U10Mo ingot (approximately 100 g each) and heated under pressurized hydrogen (0.8 MPa) at a rate of 15 °C/min up to 700 °C for one hour. After 5 min of evacuation at this temperature, the reactor was pressurized with H_2 once again to 0.8 MPa.

This procedure (activation treatment) established a clean sample surface suitable for hydriding. The reactor was cooled by taking it away from the furnace and using forced air cooling (fan) to help. After reaching room temperature under hydrogen pressure, the reactor was evacuated again (0.1 Pa) and purged with argon.

Hydrided samples were easily comminuted manually to a −125 mesh size using a stainless steel mortar. The reactor was charged with this powdered material and closed for dehydriding. The powder was heat treated under vacuum (0.1 Pa) at 400 °C. After purging with argon, the dehydrided powder was removed from the reactor inside a glove box and sieved, separating the fraction 125–44 µm. A maximum of 20 wt% of the fraction less than 44 µm was used. The powder's density of 16.87 g/cm^3 was determined using a helium pycnometer.

Fig. 7 presents the typical morphology of the U10Mo powder, and Fig. 8 presents the X-ray diffraction patterns from heat-treated (alloy before hydriding), hydrided and dehydrided powders. An amorphous-like pattern (pattern b in Fig. 8) and the reflections of the UO phase were seen after hydriding. No gamma U10Mo phase reflections were seen after hydriding, indicating that there had been a complete transformation following hydrogen absorption. The gamma phase structure was once again visible after dehydriding.

2.4. Fabrication of the fuel meats

Powder metallurgy techniques were used to manufacture the dispersion, composed of ceramic (U_3O_8) or metallic uranium composites (U_3Si_2, UMo). The fuel meat (briquette) was made by mixing the powdered fissile material with pure aluminum powder, the latter being the structural matrix material of the briquette. The three types of powders were mixed with aluminum powder using a rotary mixer. The charges used in manufacturing the briquettes were weighed and mixed individually. Homogenization was carried out at 36 rpm, 120 min under 45° inclination, and was kept the same for all types of briquettes. Fig. 9 illustrates the mixer used. Fig. 10 and Fig. 11 illustrate the morphology and size distribution, respectively, of the aluminum powder.

The composition of the pressing charges was determined based on the volume of the briquette. The masses of the fissile compounds were defined from their densities (U_3O_8, U_3Si_2, and U10Mo). The nominal dimensions of the briquette were maintained for the three types of fissile compounds, which were 59.1 × 104.2 × 4.2 mm thick with rounded corners (radius 8.4 mm). The nominal volume of the briquette was 24.93 cm^3.

The mass of aluminum was calculated to ensure a volumetric fraction of 50 % in the briquette, resulting in a mass of 33.66 g. The mass of

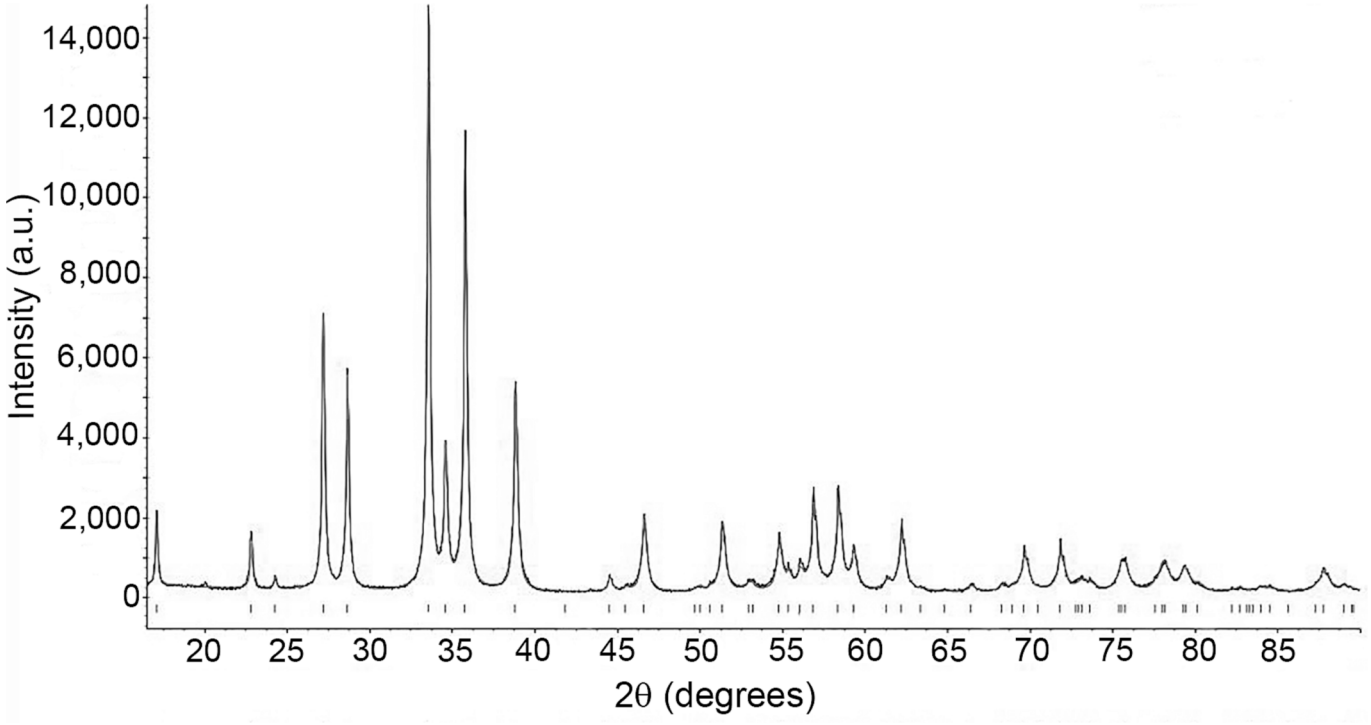

Fig. 6. X-ray diffractogram of the U_3Si_2 powder.

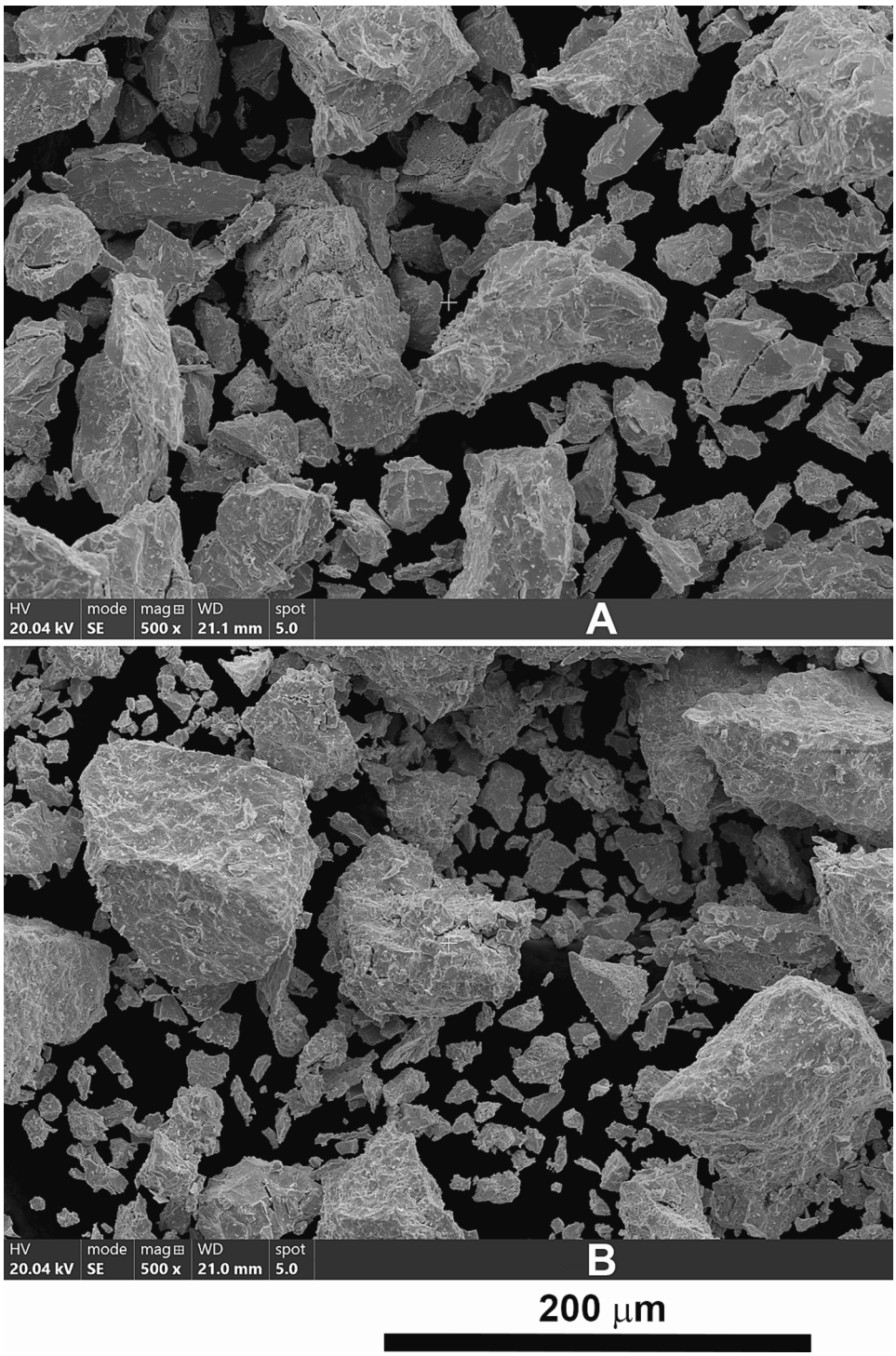

Fig. 7. SEM micrographs (secondary electrons images) of hydrided and dehydrided U10Mo powder particles: A- Hydrided particles; B- Dehydrided particles.

uranium compound powder was calculated assuming a residual porosity of 6 vol% in the fuel meat, which is typical for the production process at IPEN-CNEN/SP. The densities used for calculations were $\rho_{U3O8} = 8.35$ g/cm^3, $\rho_{U3Si2} = 12.00$ g/cm^3, and $\rho_{U10Mo} = 16.87$ g/cm^3. The uranium contents were $U_{U3O8} = 84.71$ wt%, $U_{U3Si2} = 91.37$ wt%, and $U_{U10Mo} = 89.70$ wt%. The masses of uranium compounds were: $M_{U3O8} = 91.15$ g, $M_{U3Si2} = 131.96$ g, and $M_{U10Mo} = 185.05$ g.

The pressing operation was carried out using a double-effect hydraulic press. The pressing pressure was 540 MPa for all briquettes. Table 1 shows the dimensions and the uranium density of the briquettes fabricated in the present work. Since the residual porosity of the briquettes varies slightly and the tolerance for the length and width of the briquette is ±0.2 mm, and ±0.1 mm for its thickness, the uranium density varied around the target value.

2.5. Fabrication of the fuel plates

The briquettes were degassed at 250 °C for two hours under a dynamic vacuum of 0.1 Pa. Plate fabrication followed the standard procedures adopted at IPEN-CNEN/SP, with frames and covers made from aluminum alloy 6061. The frame was 4.2 mm thick, and both the cover plates were 2.8 mm thick. The assemblies were welded and rolled using

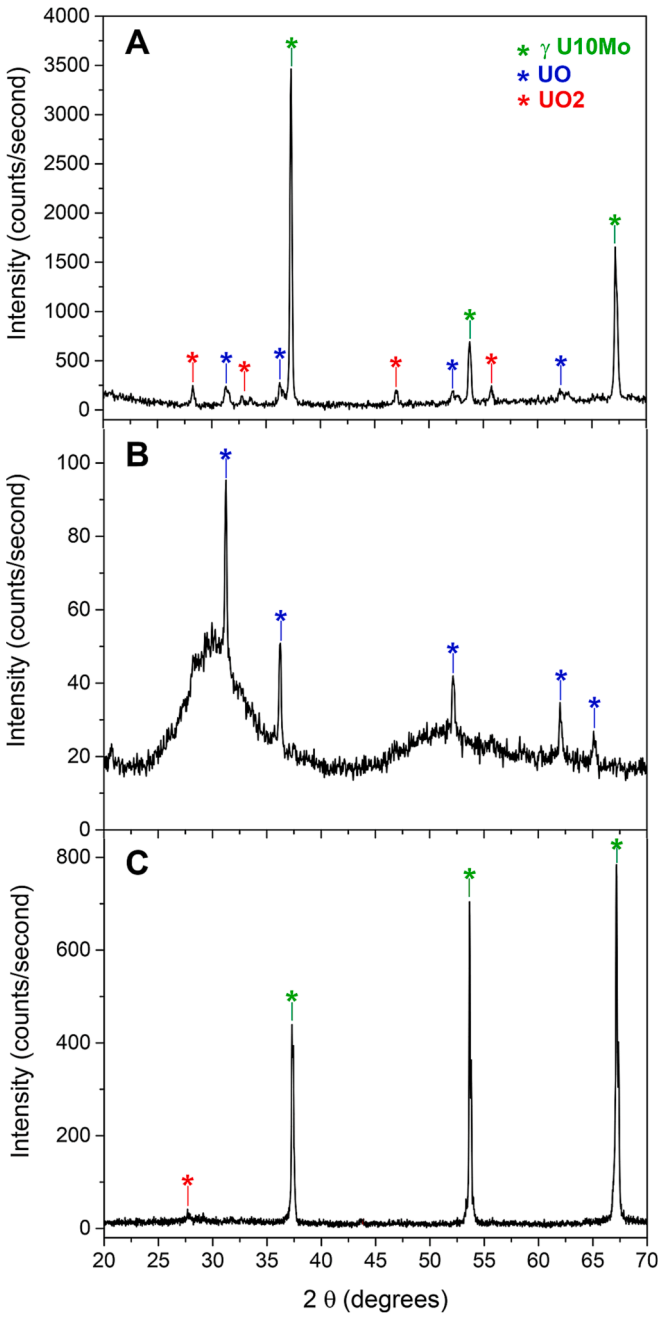

Fig. 8. X-ray diffraction patterns of as heat-treated (before hydriding) (C), hydrided (B) and dehydrided (A) samples.

the typical rolling schedule outlined in Tables 2 and 3 (Durazzo et al., 2014; Durazzo et al., 2017b). A significant amount of material remained around the briquette due to the width and length of the frame and cover plates, which allowed the frame's structural purpose to be served. The dimensions which were used consisted of 200 mm by 120 mm.

The picture frames and cover plates were labeled with a number on the outside of each top cover that corresponded to the lot number and briquette number. An "X" was used to indicate the assembly's position for proper orientation during the rolling process. Having a reference is crucial when making a fuel plate, and the "X" served as the reference edge and end of the fuel plate. To ensure good bonding quality, the frames and covers were wiped with acetone and etched using a 10 % sodium hydroxide solution and 40 % nitric acid.

The cover plates, frames, and briquettes were bonded together through hot rolling of the assemblies into plates. Prior to hot rolling, the

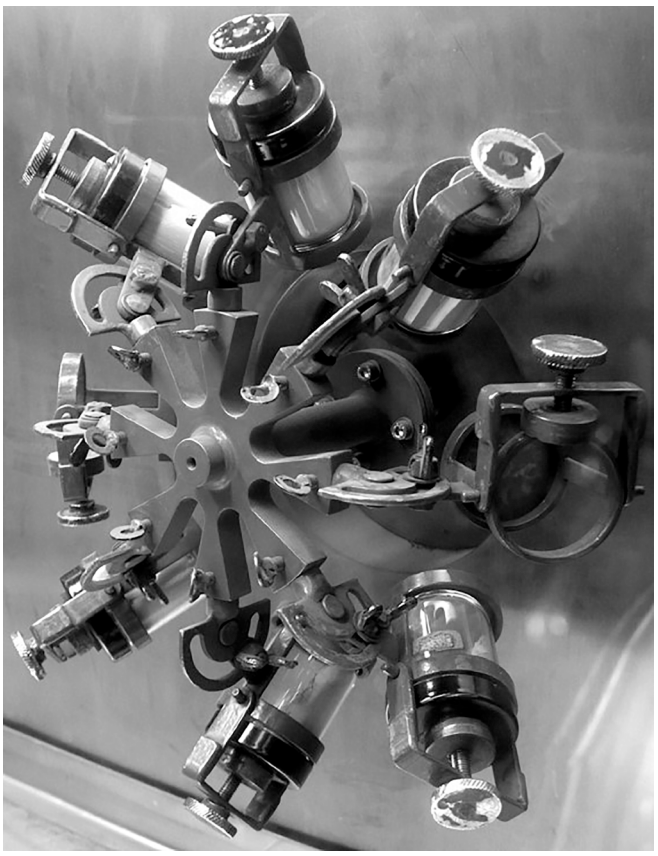

Fig. 9. Ferris wheel-type mixer for eight charge jars.

assemblies were preheated in an electric furnace equipped with a hot-air circulation blower for one hour. The hot-rolling process was carried out at a temperature of 450 °C, with the assemblies being reheated for 15 min between rolling passes. Table 2 provides the hot-rolling schedule used. The thickness of the hot-rolled plates was measured after each pass using a micrometer with a tungsten-carbide tip.

To minimize end defects and cambering, appropriate rotation was applied to the assemblies along their longitudinal and transverse axes between passes. The term "diffuse zone" refers to the end region of the fuel meat where end defects, such as "dog-bone" and "fishtail," are commonly found. This is due to the rolling process leaving the ends of the meat thicker than the middle. The longitudinal cross-section of the fuel meat with thickened ends resembles a bone, hence the name "dog-bone". To control these issues, an optimal rotation scheme was implemented during the rolling process of the fuel plates. Details on the rotation scheme during rolling are available in previous work (Durazzo et al., 2017b).

After the final hot-rolling pass, the fuel plates underwent furnace annealing at 450 °C for an hour at that temperature. Once removed from the furnace, the plates were cooled and examined for blisters. The cold-rolling process consisted of two rolling passes using a high-precision mill, with a tolerance of 0.02 mm, as outlined in Table 3. Additional information on fuel plate fabrication can be found in the literature (Durazzo et al., 2017b).

2.6. *Inspection procedures*

After cold rolling, the next step in fuel plate manufacturing involved utilizing X-ray technology to precisely outline the meat, a crucial step in preparing the fuel plate for its final specified dimensions. To facilitate subsequent flattening and accurate positioning of the fuel meat, an initial cut was performed prior to the final cutting step. In the final

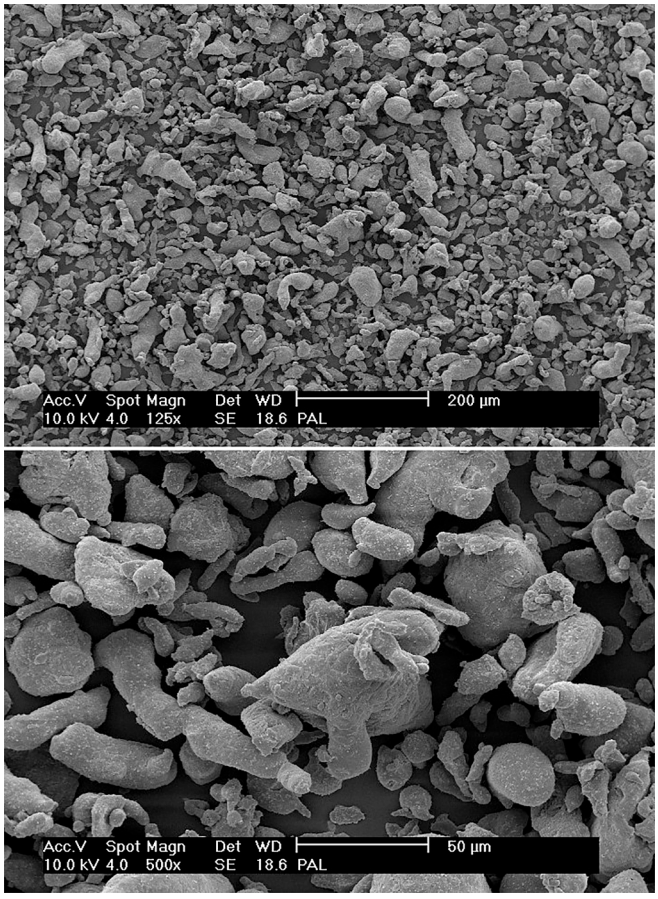

Fig. 10. SEM micrographs (secondary electrons images) of aluminum powder particles.

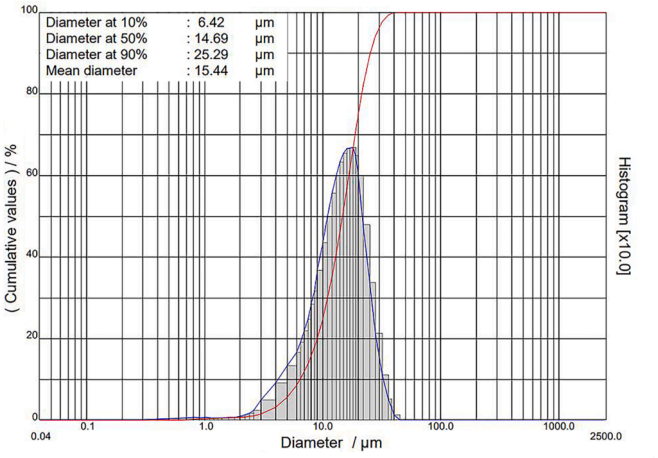

Fig. 11. Particle size distribution of the aluminum powder.

cutting stage, the fuel meat was accurately positioned using an X-ray scanner, and reference lines were marked on the pre-cut plate to locate the edges and corners of the fuel plate in its final dimensions. The final dimensions of the fuel plate were determined by measuring its length, width, and thickness. The length was measured at three positions with a caliper, achieving a precision of 0.02 mm, while the width was measured at seven positions using a micrometer with a precision of 0.01 mm. The thickness of the fuel plates was meticulously inspected at 21 positions per plate (3 × 7-point grid), employing a manual external U-shape frame micrometer with non-rotating spindles, and measured to the nearest 0.01 mm.

The length and width of the fuel meat were directly measured by an X-ray scanner, which also inspected the fuel meat's outline. The maximum width and length of the fuel meat were determined with a precision of 0.01 mm. Typically, the diffuse zone had a length ranging from 10 to 20 mm. To ensure the fuel meat was well-centered, the cladding widths at the edges and ends were directly measured on the X-ray scanner screen. The minimum widths were determined, and the differences between the widths were calculated to verify the centering of the fuel meat.

Following cold rolling, the bond integrity was assessed through a bend test. Any excess length and width of the fuel plates were trimmed during the final shearing operation. The leftover trimmings of the aluminum cladding, located directly adjacent to the final plate, were subjected to bend tests. Bend test samples were extracted from all four sides of each plate. Each sample was clamped in a test fixture and bent around a mandrel by 90 degrees in one direction, returned to 0 degrees, bent by 90 degrees in the opposite direction, and once again returned to 0 degrees. The edges of the bend test sample were visually examined for any signs of delamination.

The integrity of the fuel meat and the homogeneity of the uranium distribution inside it were inspected using an X-ray scanner. The residual porosity of all fuel plates was determined using the hydrostatic method (Archimedes principle). The microstructure, the fuel meat's thickness, and the cladding thickness were characterized using optical microscopy. The samples were prepared using conventional metallographic techniques involving embedding, sanding, and polishing. From each batch of four fuel plates fabricated from the different dispersions, one was cut to determine the thickness of the claddings and meat using metallography.

Following the usual procedure adopted by IPEN-CNEN/SP in the routine production of fuel plates, seven samples from the regions of interest were taken from each plate, as shown in Fig. 12. Samples 1, 3, 11, 13, and 9 are longitudinal, in the rolling direction, at the ends of the fuel meat and in its central zone. The samples taken from the extremity of the fuel meat (1, 3, 11, and 13) were used to measure the cladding thickness in the meat-thickening zone (dog-bone) and to characterize the terminal defect (fishtail). Samples 5 and 7 are cross-sectional and, together with sample 9, provide microstructural information about the fuel meat in the central region of the fuel plate, the defect-free region. The set of information got by the metallography of these samples is one of the main requirements for the qualification of fuel plates.

3. Results and discussion

Many aspects of fabrication are unaffected by the high uranium loading, such as the U_3O_8 and U_3Si_2 powder fabrication and the external dimensions of the fuel plate. Blister and bending tests showed satisfactory results for all high uranium-loaded fuel plates. Characteristics that are affected by high uranium loading were evaluated. The main aspects studied in this work were those that differentiate a high uranium-loaded fuel plate from that which is traditionally manufactured at IPEN-CNEN/SP with the uranium density of 3.0 gU/cm^3 (U_3Si_2). They are:

(a) U10Mo powder fabrication;
(b) dimensions of the fuel meat;
(c) homogeneity in the distribution of uranium in the fuel meat;
(d) fuel meat and cladding thicknesses;
(e) microstructure of the dispersion;
(f) end defects.

3.1. U10Mo powder fabrication

Powdering ductile gamma U-Mo alloys is a major concern when fuel manufacturing is based on the dispersion method. The primary method

Table 1
Characteristics of the briquettes.

Compound	Length (mm)	Width (mm)	Thickness (mm)	Volume (g/cm^3)	Porosity (vol%)	U Density (gU/cm^3)
	104.20	59.09	4.15	24.62	6.47	3.15
	104.18	59.10	4.16	24.68	6.47	3.14
U_3O_8	104.21	59.08	4.13	24.50	6.83	3.17
	104.17	59.13	4.12	24.45	6.47	3.17
	104.30	59.19	4.24	25.24	6.42	4.77
	104.31	59.17	4.20	24.99	6.56	4.81
U_3Si_2	104.29	59.10	4.22	25.08	6.97	4.80
	104.33	59.23	4.24	25.27	7.11	4.76
	104.15	59.15	4.15	24.63	6.21	6.74
	104.13	59.18	4.13	24.52	6.53	6.77
U10Mo	104.10	59.17	4.15	24.63	6.40	6.74
	104.13	59.17	4.12	24.45	6.67	6.79

Table 2
Typical hot-rolling schedule.

Pass	Reduction (%)	Gage (mm)	Heating Time (min)
0	0	9.20	preheating (60 min)
1	25	6.93	15
2	25	5.20	15
3	15	4.42	15
4	15	3.76	15
5	15	3.20	15
6	15	2.72	15
7	15	2.31	15
8	13	2.01	15
9	13	1.75	blistering test (60 min)

Table 3
Cold-rolling schedule.

Pass	Reduction (%)	Gage (mm)	Heating Time (min)
0	0	1.75	from hot rolling
1	7	1.63	no heating
2	6–7	1.54 – 1.50	no heating
final	0	1.54 – 1.50	final adjustment

for producing powder has been atomization, using centrifugal atomization with either the rotating disk method (Kim et al., 1997) or the rotating electrode process (Clark et al., 2007). Mechanical comminution, such as machining or grinding, is also possible (Clark and Meyer, 1998; Vacelet et al., 1999). However, due to the high cost of atomization, IPEN-CNEN/SP decided to use the hydriding-dehydriding method (Balart et al., 2000; Solonin et al., 2000; Olivares et al., 2008; Pasqualini et al., 2002; Chen et al., 2010; Yi-Fu et al., 2010), which had previously been successful in hydriding TiFe alloys for hydrogen storage (Falcão et al., 2018; Oliveira et al., 2021; Vega et al., 2019).

Fig. 8 provides X-ray diffraction patterns that show an amorphous-like pattern and reflections of the UO phase following hydriding (pattern b in Fig. 8). No gamma U10Mo phase reflections were seen, indicating a complete transformation. The gamma phase structure was visible again after dehydriding (pattern a in Fig. 8), and evidence of some oxidation was found due to the presence of the UO_2 phase.

The pycnometer density of UMo powder was 16.87 g/cm^3, which is lower than the theoretical value for U10Mo composition. The theoretical density of the U10Mo alloy can be calculated using the rule of mixtures equation based on the molar fraction (Burkes et al., 2010), resulting in 17.20 g/cm^3. Two aspects that must be considered to explain this lower value. First, our alloy's composition has slightly more Mo than the nominal. We have estimated the Mo content using an equation proposed by Dwight (Dwight, 1960) as done by Seong et al. (2000). According to Dwight, the lattice parameter of the gamma phase (diffraction analysis) varies with the Mo content (at%) by the equation a (nm) = 0.34808–0.000314 (at.% Mo). By doing so, our Mo content is 22.17 at% ($a = 0.34112$), corresponding to 10.3 wt%. The theoretical density of the U10.3Mo alloy can now be calculated at 17.11 g/cm^3. The second aspect that must be considered is related to the UO_2 content of the powder. Our pycnometer density value for the alloy powder is consistent with a UO_2

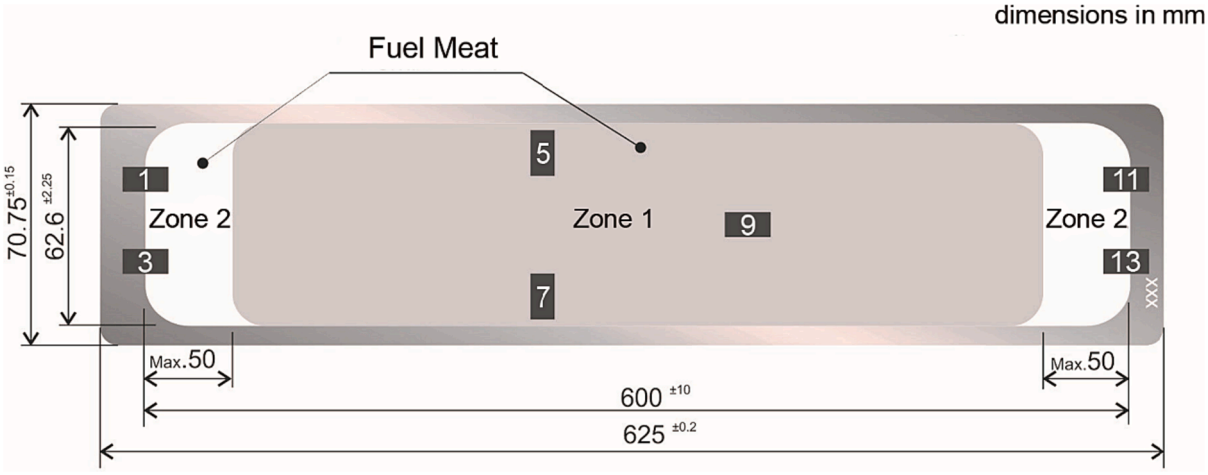

Fig. 12. Sampling plan for assessing the microstructure and thickness of the fuel plate meat.

content of about 2.5 wt%, estimated by the rule of mixtures again, which is compatible with what we see in the X-ray pattern (Fig. 8).

The hydrided and dehydrided powder particles have remarkably similar particle shapes, as seen in Fig. 7. Most particles have a regular, equiaxial shape, but some have a platelet shape. A favored crack plane may be responsible for this (Leal Neto et al., 2014). On the surface of the particles, conchoidal fracture marks, which indicate an amorphous material, were also not seen. The U10Mo particle morphology is comparable to the appearance of the U_3Si_2 particles shown in Fig. 5.

The hydriding-dehydriding procedure was successfully employed at IPEN-CNEN/SP to produce U10Mo powder for manufacturing fuel based on the U10Mo-Al dispersion. The U10Mo powder could be produced with manual grinding with appropriate granulometry. The total processing time for a batch of 3 kg of powder (safe mass) would be three days, which would enable the fuel production plant at IPEN to manufacture around 70 fuel elements annually, providing an easy supply for the RMB Reactor.

3.2. Fuel meat dimensions

After rolling, the deformation of the fuel meats showed a behavior very similar to that of the traditional fuel manufactured by the IPEN-CNEN/SP. The widening and elongation during rolling were very similar to those usually observed. Table 4 displays the dimensions of the fuel meats of the high uranium-loaded fuel plates manufactured in the present work. The length and width values of the fuel meat satisfy the current IEA-R1 research reactor specification, allowing for seamless adaptation to the fuel plate thickness. This maintained the flexibility to vary the thickness of the fuel plate to keep the fuel meat dimensions within specification. The rolling operation presented no difficulties related to the high uranium concentration in the fuel plates.

The uranium densities of the U_3O_8-Al fuel plates are significantly lower than the target value of 3.2 gU/cm^3, due to the high residual porosity observed in the meat of finished plates. This porosity is considerably higher than the typical value of around 9 % in volume observed in low-concentration U_3O_8-Al fuel. The high porosity indicates an intense fragmentation of the U_3O_8 particles, which is expected due to the higher interaction between the U_3O_8 particles during meat deformation with the increase in the volumetric fraction.

A similar observation is valid for the high uranium-loaded U_3Si_2-Al and U10Mo-Al fuel plates but with much less intensity. The residual porosity also increases with the meat deformation but in a much less pronounced way. Particle fragmentation also occurs, but it is much less intense than that observed in U_3O_8-Al dispersions. Note that the particle fragmentation for the U10Mo-Al dispersion is slightly smaller than for the U_3Si_2-Al, resulting in a consistent decrease in residual porosity. The uranium density is little affected by the rolling operation for U_3Si_2 and U10Mo due to their low fragmentation, as shown in Tables 1 and 4.

The fuel meat's residual porosity varies from fabricator to fabricator, depending on various factors, such as the amount of fines (44 μm) in the powder, the rolling schedule, the strength of the aluminum alloy used for the frames and covers, the rolling temperature, the relationship between the size of the compact and the size of the cavity in the frame, and most importantly, the amount of cold reduction (Matos and Snelgrove, 1992).

3.3. Homogeneity in the distribution of uranium in the fuel meat

X-ray radiographs of the high uranium-loaded fuel plates showed a good distribution of uranium in the fuel meat, meeting the acceptable standards for visual inspection and comparison with a standard. The radiographs in Fig. 13 demonstrate good homogeneity for all the manufactured plates, but dark and light regions at the meat's ends suggest abnormal thickening of the meat in this region (dog-bone). However, all types of fuels examined met current thicknesses specifications for meat and cladding.

3.4. Fuel meat and cladding thicknesses

The cladding thickness is a crucial fuel plate specification that prevents the fuel meat from being exposed to the reactor environment. The thickening of the meat of the fuel plate's ends is a phenomenon resulting from the difference in mechanical properties of the briquette and the cladding, leading to a decrease in cladding thickness in this region (dog-bone), which is inevitable and one of the most critical defects regarding fuel plate qualification since the minimum cladding thickness in this zone must meet the specification.

Table 5 presents the results of measuring the thickness of the meat and claddings of fuel plates with high uranium loadings. The specification divides the meat region into two zones. Zone 1, the central zone, requires a minimum cladding thickness of 0.30 mm and a range of 0.76 $\pm$ 0.05 mm for meat thickness. Zone 2, also called the end defects zone, extending 50 mm from the meat's end, permits a minimum cladding thickness of 0.25 mm and a maximum meat thickness of 1.07 mm. All high uranium-loaded fuel plates easily met the thickness specifications of the claddings and meat.

Table 4
Dimensional data on the fuel meats of high-loaded fuel plates.

Compound	Fuel Plate Thickness (mm)	Fuel Meat Length (mm)	Fuel Meat Width (mm)	Fuel Meat Volume (g/cm^3)	Fuel Meat Porosity (vol%)	U Density (gU/cm^3)
Specification IEA-R1 Fuel (3.0 gU/cm^3)	1.47–1.57	590–610	60.35–65.00	Not Specified	7 to 8 (typical)	3.00
	1.53	600.5	61.51	25.44	14.39	3.05
	1.54	595.0	61.79	25.44	14.39	3.05
U_3O_8	1.53	598.5	61.73	25.52	14.35	3.04
	1.52	605.0	61.97	25.44	14.21	3.05
	1.52	603.0	61.20	25.32	9.33	4.75
	1.53	601.0	61.24	25.16	9.34	4.78
U_3Si_2	1.51	604.0	61.12	25.27	9.48	4.76
	1.52	602.0	61.31	25.32	9.34	4.75
	1.51	601.5	61.10	24.70	8.71	6.72
	1.50	602.0	61.22	24.63	8.81	6.74
U10Mo	1.52	600.5	60.95	24.77	8.70	6.70
	1.51	601.0	61.08	25.55	8.75	6.76

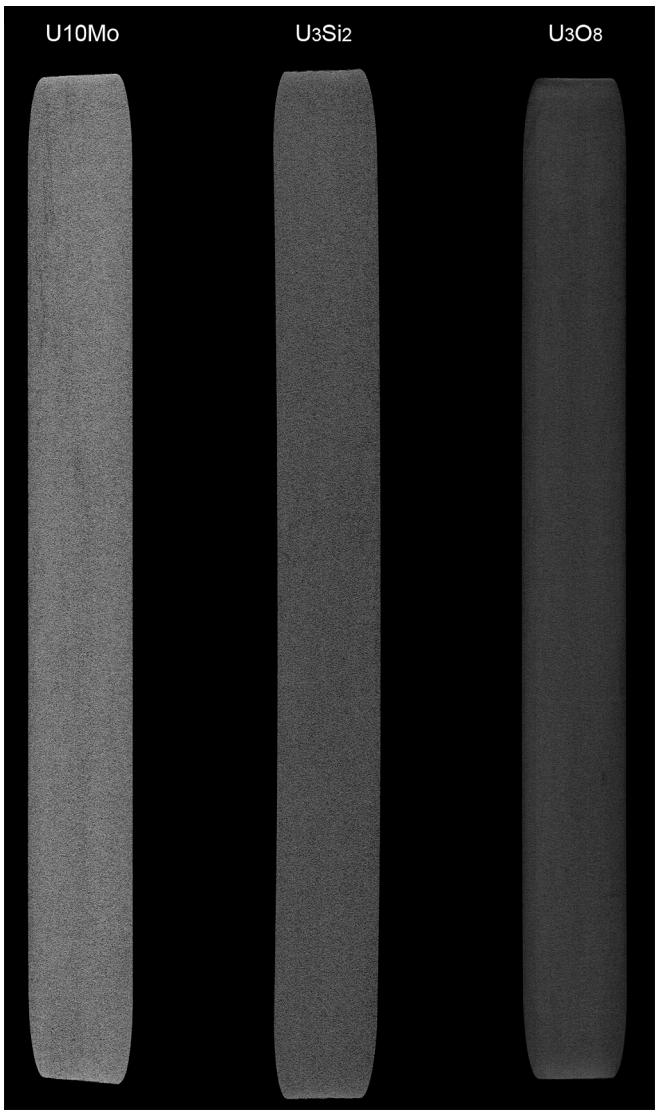

Fig. 13. X-Ray radiographs illustrating the homogeneity of uranium distribution in the meat of fabricated fuel plates.

Table 5
Values for cladding and meat thicknesses.

	Zone 1		Zone 2	
	Meat| (mm) min–max	Cladding (mm) min–max	Meat (mm) min–max	Cladding (mm) min–max
U_3O_8	0.78–0.79	0.37–0.38	0.84–0.89	0.30–0.31
U_3Si_2	0.75–0.76	0.37–0.39	0.78–0.88	0.32–0.37
U10Mo	0.73–0.76	0.37–0.39	0.77–0.88	0.31–0.35

Preliminary tests showed that the U_3Si_2-Al dispersion-based fuel plates exceeded the maximum meat thickness value specified in Zone 1 (0.81 mm). The thickness values of the claddings in Zone 1, despite being within the specification (minimum of 0.30 mm), were smaller than typical production values observed in traditional fuels manufactured at IPEN-CNEN/SP, which ranged from 0.38 and 0.40 mm. This behavior was related to the penetration of large U_3Si_2 particles into the cladding, caused by the increase in the volumetric fraction of U_3Si_2, which hindered the accommodation of U_3Si_2 particles in the meat (especially the larger ones) because of the low volume of the aluminum matrix, forcing the penetration of the particles into the cladding. Fig. 14 illustrates this effect. The maximum particle size used in all dispersions has been then reduced 150 μm (former value) to 125 μm to avoid this problem, and the results presented in Table 5 were satisfactory. The behavior of the U10Mo-Al dispersion was very similar to the U_3Si_2-Al.

The thickness of the claddings and meats were measured by destroying the thinnest plates (1.50 mm for U10Mo-Al, 1.51 mm for U_3Si_2-Al, and 1.52 mm for U_3O_8-Al) as shown in Table 4. This method yielded conservative estimates for the thickness of the cladding. The fuel plates typically manufactured at IPEN-CNEN/SP have a thickness of 1.54 mm, but plates with a maximum of 1.57 mm can be produced routinely without any difficulty. Therefore, the cladding thickness values reported in Table 5 can be increased further.

3.5. Microstructure of the dispersion

To increase the uranium loading on fuel plates that used a U-Al alloy with a uranium content limited to 18 wt%, the dispersion fuel concept emerged in 1955 (Weber and Hirsch, 1955; Howe, 1955; Billington, 1955). The concept's basic principle is to preserve the fuel's pre-irradiation properties after irradiation by controlling the microstructure. When exposed to radiation, a dispersion meat's behavior is ultimately determined by its microstructure. Some of the fission fragments will recoil into the matrix phase of the dispersion even though they are born in the uranium compound particles. For instance, aluminum has a 13.7 μm fragment recoil range (Weber and Hirsch, 1955). The magnitude of the irradiation damage in the dispersion depends on how much fission products affect the matrix. To leave a continuous fission product-free matrix region around the damage zone, a dispersion tries to concentrate the irradiation damage in the dispersed phase and a highly localized region surrounding the dispersed fissile particle.

An ideal dispersion must meet certain design goals, including large-dispersed particle size compared to the fission product recoil range (White et al., 1957), uniform particle dispersion in the aluminum matrix, a continuous phase of a matrix with the highest volume fraction possible, and a high uranium density fissile phase (to retain fission fragments on their own). The discussion of microstructures will be founded on this concept.

Fig. 15 shows the microstructure of the high uranium-loaded U_3O_8-Al dispersion. The figure clearly shows the intense fragmentation of U_3O_8 particles, resulting in their alignment in a "stringering" pattern. The low-magnification micrograph provides a better illustration of the stringering, with elongated voids visible in the rolling direction. These voids may have been formed due to the drag of U_3O_8 particles through

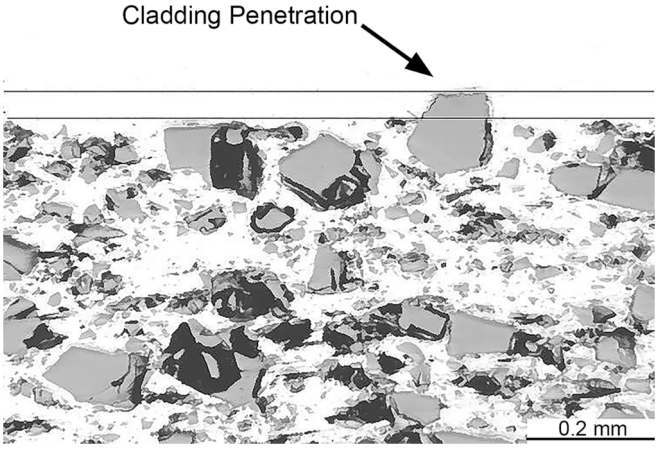

Fig. 14. Optical micrograph illustrating U_3Si_2 particles penetrating the cladding, decreasing its effective thickness.

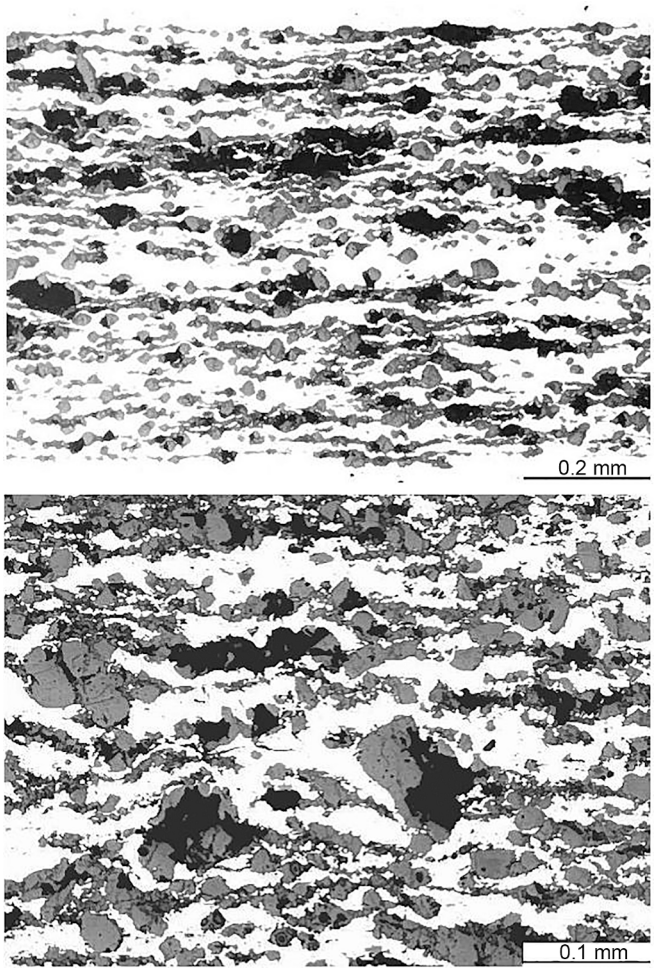

Fig. 15. Optical micrographs illustrating the meat microstructure of U_3O_8-Al fuel plates.

the flow of the aluminum matrix during deformation. Therefore, it can be assumed that U_3O_8 particles fragment and are dragged during rolling, creating voids. With an increase in uranium loading, the formation of voids also increases, both due to fragmentation and dragging. The volume fraction of the aluminum matrix also decreases simultaneously, making it difficult to eliminate the voids during hot rolling.

The microstructure thus explains the high residual porosity present in the meat, as shown in Table 4. The usual residual porosity for this fuel type with 2.3 gU/cm^3, fabricated at IPEN-CNEN/SP, is 9 % in volume. As a result, the uranium densities for the U_3O_8-Al fuel plates are significantly lower than the target value of 3.2 gU/cm^3.

Hobson and Leitten (1967) noticed that the fragmentation of U_3O_8 particles during rolling depends on the density and shape-related fragmentation resistance of the particles. Other factors, such as rolling temperature, reduction per pass, and particle spacing, can also affect fragmentation. Since the characteristics of the U_3O_8 powder used to manufacture all samples and the rolling process were kept constant, the spacing between the particles, which is determined by on the uranium loading of the sample or its U_3O_8 concentration, is the sole factor that affects fragmentation. Therefore, an increase in fragmentation was expected as the uranium loading increased.

Despite the high density of the U_3O_8 powder used in this work (8.35 g/cm^3), the SEM micrograph shown in Fig. 3 reveals that the particle is not cohesive, as confirmed by the SEM micrograph with higher magnification shown in Fig. 16. Although the granules were sintered at 1400 °C for 6 h, their morphology suggests low resistance to fragmentation. The sintered particle shows the interface ("necks") between the original particles before sintering. During rolling, the particles are expected to fracture at these interfaces. Fragmentation is intensified when the interaction between particles increases with the increase in the volumetric fraction of U_3O_8. An alternative to minimize this problem would be to sinter U_3O_8 pellets and grind them instead of sintering the granules. Fig. 17 illustrates the morphology of the U_3O_8 particles obtained by sintering pellets and subsequent grinding. Note the absence of "necks" interfaces, with an aspect of continuity. The appearance of the particle is comparable to that of the U_3Si_2 particle (Fig. 5).

Fig. 18 shows the microstructure of the high uranium-loaded U_3Si_2-Al dispersion. Unlike in the case of U_3O_8, intense fragmentation of U_3Si_2 particles is not immediately noticeable in this microstructure. However, some mild stringering is evident in Fig. 18. In a previous study, Durazzo et al., (2017b) conducted a qualitative examination of particle fragmentation in a U_3Si_2-Al dispersion with a uranium density of 3.0 gU/cm^3. They observed the beginning of U_3Si_2 particle fragmentation during the first hot-rolling pass, but without pronounced separation of the fragments. Porosity formation was found to occur due to fragmentation, and although porosity did not increase significantly during hot rolling, the number of fine U_3Si_2 particles slightly increased. Cold rolling, on the other hand, resulted in more pronounced fragmentation of U_3Si_2 particles and a noticeable decrease in the maximum particle size. Residual porosity also appeared to slightly increase. Ongoing work aims to quantitatively study the fragmentation of U_3Si_2 particles during rolling.

Fig. 19 shows the microstructure of the high uranium-loaded U10Mo-Al dispersion. The microstructural appearance of the dispersion after rolling is comparable to the U_3Si_2-Al dispersion, with a lower apparent level of pores. The existing pores appear to be associated with recesses on the surface of the particles, and the marks on the particle surface suggest some degree of cracking. However, no stringering is visible. In contrast to U_3Si_2-Al dispersion microstructures, U10Mo particles do not appear to fragment when subjected to rolling; rather, they become deformed and elongated in the rolling direction. Additionally, there is a lower proportion of fine particles visible in the microstructure of U10Mo dispersions, indicating that the U10Mo particles tend to deform rather than fragment.

Ideally, a dispersion should have isolated particles of fissile material, with a continuous aluminum matrix surrounding each particle. In the case of the U_3Si_2-Al and U10Mo-Al dispersions, the microstructural appearance can be regarded as satisfactory based on the theoretical assumptions of an ideal dispersion. Nonetheless, the absence of specific standards for the microstructural characteristics of the fuel plate meat means that the assessment is subjective. It depends on the experience and common sense of each manufacturer, supported by irradiation tests.

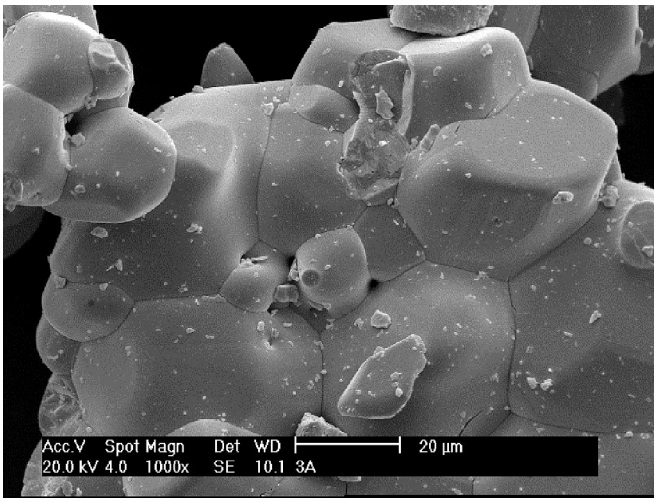

Fig. 16. SEM micrograph (secondary electrons image) of a U_3O_8 powder particle showing the interfaces.

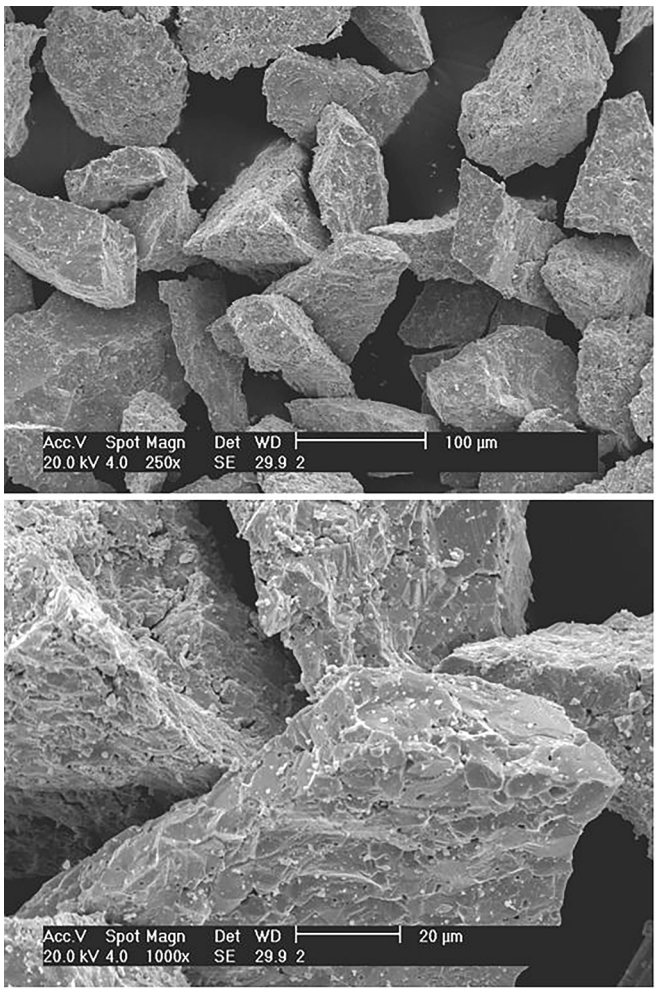

Fig. 17. SEM micrographs (secondary electrons images) of a U_3O_8 powder particle prepared by sintering and grinding U_3O_8 pellets.

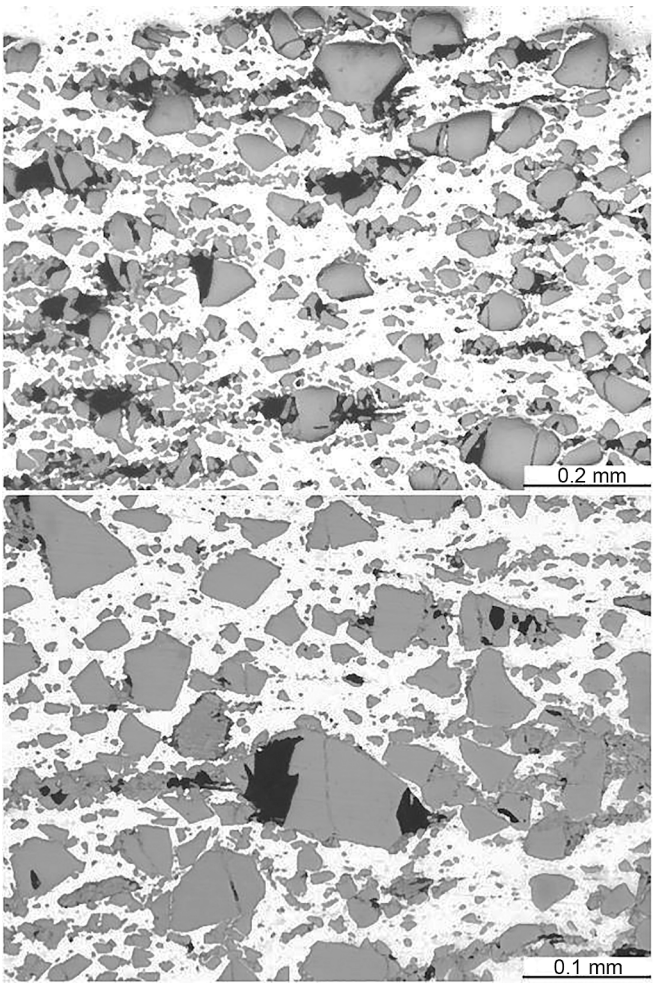

Fig. 18. Optical micrographs illustrating the meat microstructure of U_3Si_2-Al fuel plates.

Although there are no quantitative requirements to disqualify the microstructure of U_3O_8-Al, the microstructural appearance of high uranium-loaded U_3O_8-Al meat deviates from the theoretical requirements for a good quality dispersion.

3.6. End defects

Besides the thickening at the end of the meat (dog-bone), there is another important terminal defect known as "fishtail", which is related to the shape of the fuel plate's meat. Although this defect is not specified, the only requirement is that it does not exceed the end defects zone, or Zone 2, with a length of 50 mm. The geometry of this defect is considered normal for all high uranium-loaded dispersion fuel plates manufactured, and it is illustrated in Fig. 20. This type of end defect is typical of traditional fuel plates manufactured at IPEN-CNEN/SP and is common in this type of manufacturing process.

The fishtail defect length was 14 mm for the U_3O_8-Al dispersion, 20 mm for the U_3Si_2-Al dispersion, and 30 mm for the U10Mo-Al dispersion, all of which fall within the maximum allowed value of 50 mm. However, the value for the U10Mo-Al dispersion is notably higher than the typical range of 10–20 mm observed in the manufacturing of fuel plates with 3.0 gU/cm^3. This discrepancy can be attributed to the difference in thickness between the briquette and the frame, which can influence the occurrence of fishtail defects. When the briquette thickness greatly exceeds the frame thickness, this defect becomes more pronounced. Currently, the specification for the frame and briquette thickness is set at 4.2 ± 0.1 mm, which can lead to a difference of up to 0.2 mm in thickness. To reduce the length of the fishtail defect, the specification tolerance for the thickness of the frame plate can be decreased to 4.20 ± 0.05 mm. This proposal would be a good starting point for the specification of the frame and briquette thickness.

4. Conclusions

Through this work, a substantial amount of experience was gained in manufacturing high uranium-loaded full-size plates, primarily for UMo-Al dispersion fuel, validating the previous procedures used for mini-plates. Successful production was achieved using high-uranium-loaded U10Mo-Al and U_3Si_2-Al dispersions, utilizing the same processes as those used for low-uranium-loaded fuel plate production at IPEN-CNEN/SP. The UMo powder with the required granulometry was produced using simple manual grinding, and the HMD technique generated powder particles suitable for use as fuel.

The distribution of uranium in the meat of all types of fuel plates with high uranium loading was homogeneous, with no observed bonding failures. The final dimensions of the meat of the finished fuel plate met the specification without changes to the thermomechanical treatment adopted in routine production. The thicknesses of the fuel meat and claddings of the fuel plates for all types of high uranium-loaded dispersions fell well within the specification.

The microstructures of the meats of the U_3Si_2-Al and U10Mo-Al dispersions were considered adequate. However, for U_3O_8-Al high uranium loaded dispersion fuel, intense fragmentation of U_3O_8 particles

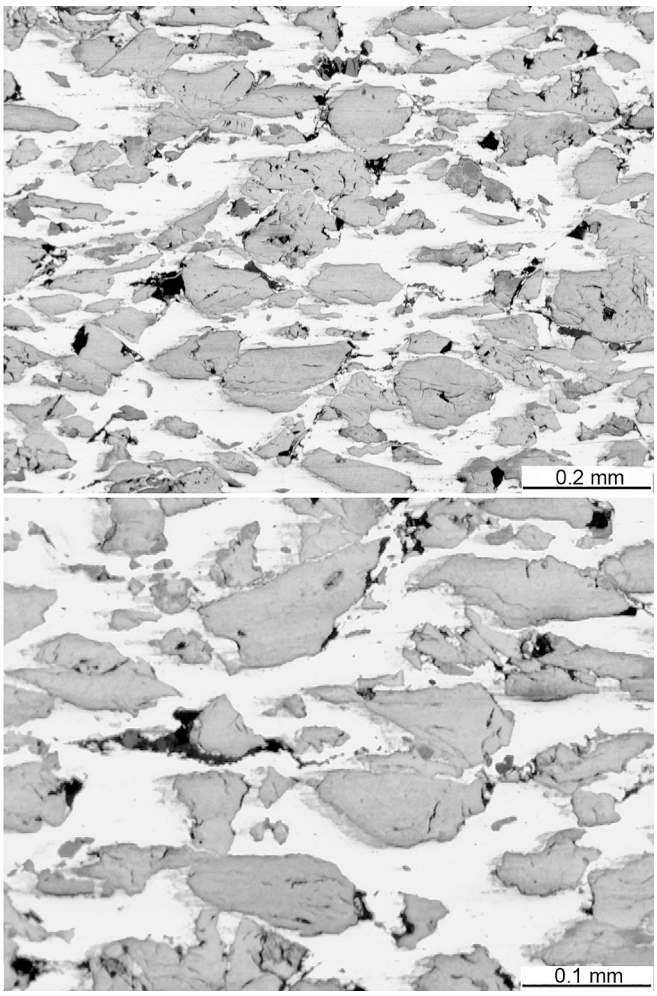

Fig. 19. Optical micrographs illustrating the meat microstructure of U10Mo-Al fuel plates.

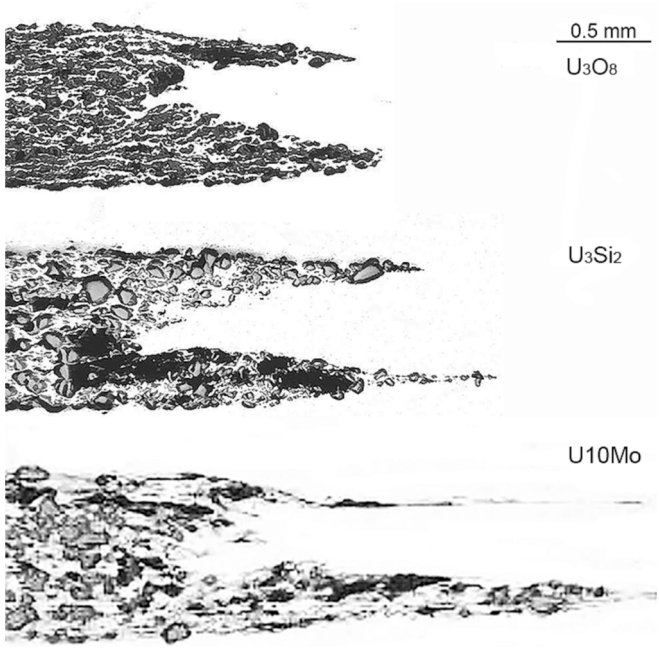

Fig. 20. Optical micrographs illustrating the end defects of fuel meats.

and pronounced "stringering" (alignment of the fragments in the rolling direction) were observed, indicating that the microstructure did not meet the theoretical requirements of good quality dispersion. This microstructure issue could possibly be addressed by changing the U_3O_8 powder production process by sintering U_3O_8 pellets instead of granules. However, despite the greater simplicity of the U_3O_8 powder manufacturing process, this fuel type should be discontinued at IPEN-CNEN/SP, due to the limitations on the uranium density.

Three high uranium-loaded U_3Si_2-Al dispersion fuel plates (4.78–4.79 gU/cm^3) were fabricated to be irradiated in the IEA-R1 reactor. Studies are underway to investigate the use of silicon addition in the aluminum powder to control the reaction of UMo particles with the aluminum matrix of the dispersion.

CRediT authorship contribution statement

Michelangelo Durazzo: Writing – review & editing. **Jose Antonio Batista Souza:** Investigation, Resources, Data curation. **Elita Fontenele Urano de Carvalho:** Visualization. **Thomaz Augusto Guisard Restivo:** Methodology, Validation, Data curation. **Frederico Antonio Genezini:** Methodology, Validation. **Ricardo Mendes Leal Neto:** Methodology, Validation, Writing – review & editing.

Declaration of competing interest

The authors declare that they have no known competing financial interests or personal relationships that could have appeared to influence the work reported in this paper.

Data availability

Data will be made available on request.

Acknowledgments

The authors are grateful to CNPq (National Council for Scientific and Technological Development) for the research grant 309826/2021-7 provided for this work. The authors would also like to thank São Paulo Research Foundation (FAPESP) for the research grants 2021/14331-5, 2011/13849-9, 2007/50018-2, and 2007/07769-7.

References

Nuclear Energy Agency, 2019. The Supply of Medical Radioisotopes: 2019 Medical Isotope Demand and Capacity Projection for the 2019-2024 Period. OECD Publishing, Paris, 2019. NEA/SEN/HLGMR(2019)1 (available at https://www.oecd-nea.org/med-radio/docs/sen-hlgmr2019-1.pdf).

Balart, S., Bruzzoni, P., Granovsky, M., Gribaudo, L., Hermida, J., Ovejero, J., Rubiolo, G., Vicente, E., 2000. U-Mo alloy powder obtained by a hydride-dehydride process: in Proceedings of the 2000 International Meeting on Reduced Enrichment for Research and Test Reactors, Las Vegas, Nevada, October 1-6, 2000. (available at https://www.osti.gov/etdeweb/servlets/purl/20432977).

Beaver, R. J., Patriarca, P., Adamson, G. M., 1964. Procedures for fabricating aluminum-base ATR fuel elements. Oak Ridge, Tennessee, 1964. ORNL-3632.

Billington, D. S., 1955. Radiation damage in reactor materials: in Proceedings of the International Conference on the Peaceful Uses of Atomic Energy, Geneve, Switzerland, August 8-20, 1955.Paper No. P/744.

Burkes, D. E., Mickum, G. S., Wachs, D. M., 2010. Thermophysical properties of U-10Mo alloy. Idaho National Laboratory, Idaho Falls, Idaho, November 2010. INL/EXT-10-19373. (available at https://inldigitallibrary.inl.gov/sites/sti/sti/4702554.pdf).

Chen, M., Yi-fu, X., Jing, W., Jia, J., Zhang, P., 2010. Characterization of γ-U–10 wt.%Mo alloy powders obtained by hydride-milling-dehydride process. J. Nucl. Mater. 400, 69–72. https://doi.org/10.1016/j.jnucmat.2010.02.011.

Clark, C. R., Meyer, M. K., 1998. Fuel powder production from ductile uranium alloys: In: Proceedings of the 1998 International Meeting on Reduced Enrichment for Research and Test Reactors, São Paulo, Brazil, October 18-23,1998. (available at https://www.osti.gov/servlets/purl/11072).

Clark, C. R., Muntifering, B. R., Jue, J. F., 2007. Production and characterization of atomized U-Mo powder by the rotating electrode process: In: Proceedings of the 2007 International Meeting on Reduced Enrichment fot Research and Test Reactors, Prague, Czech Republic, September 23-27, 2007. (available at https://core.ac.uk/download/pdf/71325333.pdf).

Cunningham, E., Boyle, E. J., 1955. MTR-Type fuel elements. International Conference on Peaceful Uses of Atomic Energy. Geneva, 8-20 August, V. 9, 1955, pp. 203-7.

Durazzo, M., Leal Neto, R. M., Marques, J. R. O., 2014. Fabrication procedures for manufacturing UMo-Al dispersion fuel. In: Proceedings of the 2014 International Meeting on Reduced Enrichment fot Research and Test Reactors, Vienna, Austria, October 12-16, 2014. (available at https://www.rertr.anl.gov/RERTR35/index.shtml).

Durazzo, M., Riella, H.G., 2015. Procedures for Manufacturing Nuclear Research Reactor Fuel Elements. OmniScriptum GmbH & Co, KG, Saarbrücken, Germany.

Durazzo, M., Saliba-Silva, A.M., Martins, I.C., Urano de Carvalho, E.F., Riella, H.G., 2017a. Manufacturing low enriched uranium metal by magnesiothermic reduction of UF_4. Ann. Nucl. Energy 110, 874–885. https://doi.org/10.1016/j.anucene.2017.07.033.

Durazzo, M., Vieira, E., Urano de Carvalho, E.F., Riella, H.G., 2017b. Evolution of fuel plate parameters during deformation in rolling. J. Nucl. Mater. 490, 197–210. https://doi.org/10.1016/j.jnucmat.2017.04.018.

Durazzo, M., Conturbia, G.L.C.R., Urano de Carvalho, E.F., 2021. Increasing productivity in the manufacture of UAl_2–Al dispersion-plate targets for Mo-99 production. Prog. Nucl. Energy 140, 103920. https://doi.org/10.1016/j.pnucene.2021.103920.

Durazzo, M., Souza, J.A.B., Ianelli, R.F., Takara, E.M., Garcia Neto, J.S., Saliba-Silva, A. M., Urano de Carvalho, E.F., 2022. Manufacturing LEU-foil annular target in Brazil. Ann. Nucl. Energy 165, 108646. https://doi.org/10.1016/j.anucene.2021.108646.

Dwight, A.E., 1960. The uranium-molybdenum equilibrium diagram below 900° C. J. Nucl. Mater. 2, 81–87. https://doi.org/10.1016/0022-3115(60)90028-3.

Falcão, R.B., Dammann, E.D.C.C., Rocha, C.J., Durazzo, M., Ichikawa, R.U., Martinez, L. G., Botta, W.J., Leal Neto, R.M., 2018. An alternative route to produce easily activated nanocrystalline TiFe powder. Int. J. Hydrogen Energy 43, 16017–16116. https://doi.org/10.1016/j.ijhydene.2018.07.027.

Hobson, D.O., Leitten Jr., C.P., 1967. Characterization of U_3O_8 Dispersions in Aluminum. Oak National Lab, Oak Ridge, Tn. ORNL-TM-1962. (available at https://www.osti.gov/servlets/purl/4452516).

Howe, J. P., 1955. The metallurgy of reactor fuels. In: Proceedings of the International Conference on the Peaceful Uses of Atomic Energy, Geneve, Switzerland, August 8-20, 1955.Paper No. P/825.

Kaufman, A.R., 1962. Nuclear Reactor Fuel Elements, Metallurgy and Fabrication. Interscience, New York, N.Y.

Kim, K.H., Lee, D.B., Kim, C.K., Hofman, G.E., Paik, K.W., 1997. Characterization of U-2 wt% Mo and U-10 wt% Mo alloy powders prepared by centrifugal atomization. J. Nucl. Mater. 245, 179–184. https://doi.org/10.1016/S0022-3115(97)00011-1.

Knight, R. W., Morin, R. A., 1999. Fabrication procedures for manufacturing High Flux Isotope Reactor fuel elements II. Oak Ridge, Tenn., Oak Ridge National Lab., December 1999. ORNL-6852. https://doi.org/10.2172/757311.

Knight, R. W., Binns, J., Adamson Jr., G. M., 1968. Fabrication procedures for manufacturing high flux isotope reactor fuel elements. Oak Ridge, Tenn., Oak Ridge National Lab., June 1968. ORNL–4242. https://doi.org/10.2172/4501160.

Kucera, W. J., Leitten, C. F., Beaver, R. J., 1963. Specifications and procedures used in manufacturing U_3O_8-aluminium dispersion fuel elements for Core I of the Puerto Rico Research Reactor. Oak Ridge, Tenn., Oak Ridge National Lab., 1963. ORNL–3458.

Leal Neto, R.M., Rocha, C.J., Urano de Carvalho, E., Riella, H.G., Durazzo, M., 2014. Investigation of powdering ductile gamma U-10 wt%Mo alloy for dispersion fuels. J. Nucl. Mater. 445, 218–223. https://doi.org/10.1016/j.jnucmat.2013.11.014.

Matos, J. E., Snelgrove, J. L., 1992. Selected thermal properties and uranium density relations for alloy, aluminide, oxide, and silicide fuels. Research reactor core conversion guidebook. V. 4: Fuels (Appendices I-K). Appendix I-1.1. 13-29. International Atomic Energy Agency. Vienna. 1992. IAEA-TECDOC-643. (available at https://www-pub.iaea.org/MTCD/Publications/PDF/te_643v4_prn.pdf).

Obadia, I.J., Perrotta, J A., 2010. A sustainability analysis of the Brazilian Multipurpose Reactor Project. In: International Topical Meeting on Research Reactor Fuel Management RRFM 2010, Marrakech, Morocco, 21-25 March, 2010 (available at Microsoft Word - RRFM2010_Full text.doc (iaea.org).

Olivares, L., Marin, J., Lisboa, J., Pesenti, H., 2008. Powder production of uranium-molybdenum-metal alloys applying hydride-dehydride methodology. In: Proceedings of the 2008 International Meeting on Reduced Enrichment for Research and Test Reactors, Washington, D.C., October 5-9, 2008. (available at: http://www.rertr.anl.gov/RERTR30/pdf/S10-5_Olivares.pdf).

Oliveira, V.B., Beatrice, C.A.G., Leal Neto, R.M., Silva, W.B., Pessan, L., Botta, W.J., Leiva, D.R., 2021. Hydrogen absorption/desorption behavior of a cold-rolled tife intermetallic compound. Mater. Res. 24, 1–9. https://doi.org/10.1590/1980-5373-MR-2021-0204.

Pasqualini, E. E., Garcia, J. H., Lopez, M., Cabanillas, E., Adelfang, P., 2002. Powder Production of U-Mo Alloy by HMD Process.(Hydriding-Milling-Dehydriding). In: 6th International Topical Meeting on Research Reactor Fuel Management (RRFM 2002), European Nuclear Society, Ghent, Belgium, April 21-25. pp. 183-187. (available at 20344211 (osti.gov).

Perrotta, J.A., Obadia, I.J., 2011. The RMB Project development status. In: Proceeding of International Conference on Research Reactors: Safe Management and Effective Utilization. Session C: New Research Reactor Projects. 14-18 November 2011, Rabat, Morocco. Proceedings series. International Atomic Energy Agency. 2012. STI/PUB/1575 978-92-0-184610-5 (available at https://www-pub.iaea.org/MTCD/Publications/PDF/P1575_CD_web/datasets/abstracts/C6Perrotta.html).

Perrotta, J.A., Soares, A.J., 2014. RMB: The new Brazilian Multipurpose Research Reactor. In: International Topical Meeting on Research Reactor Fuel Management RRFM 2014, Ljubljana, Slovenia, 20 March – 3 April, P. 394-401, 2014 (available at https://www.euronuclear.org/download/proceedings-rrfm-2014/).

Seong, B.S., Lee, C.H., Lee, J.S., Shim, H.S., Lee, J.H., Kim, K.H., Kim, C.K., Em, V., 2000. Neutron diffraction study of U–10 wt% Mo alloy. J. Nucl. Mater. 277, 274–279. https://doi.org/10.1016/S0022-3115(99)00198-1.

Silva, A.T., Terremoto, L.A.A., Silva, J.E.R., Almeida, C.T., Damu, M.A., Umbehaun, P.E., Yamaguchi, M., 2008. Qualification program of research fuels manufactured at IPEN-CNEN/SP. Prog. Nucl. Energy 50, 795–799. https://doi.org/10.1016/j.pnucene.2007.08.007.

Solonin, M., Vatulin, A. V., Stetsky, Y. A., Trifonov, Y. I., Rogozkin, B. D., 2000. Development of the method of high density fuel comminution by hydride-dehydride processing. In: Proceedings of the 2000 International Meeting on Reduced Enrichment for Research and Test Reactors, Las Vegas, Nevada, October 1-6, 2000. (available at https://inis.iaea.org/search/search.aspx?orig_q=RN:42024822).

Vacelet, H., Sacristan, P., Languille, A., Lavastre, Y., Grasse, M., 1999. Irradiation of full size UMo plates. In: Proceedings of the 1999 International Meeting on Reduced Enrichment for Research and Test Reactors, Budapest, Hungary, October 3-8, 1999. (available at https://inis.iaea.org/collection/NCLCollectionStore/_Public/35/015/35015905.pdf).

Vega, L.E.R., Leiva, D.R., Leal Neto, R.M., Silva, W.B., Silva, R.A., Ishikawa, T.T., Kiminami, C.S., Botta, W.J., 2019. Improved ball milling method for the synthesis of nanocrystalline TiFe compound ready to absorb hydrogen. Int. J. Hydrogen Energy 45, 2084–2093. https://doi.org/10.1016/j.ijhydene.2019.11.035.

Weber, C. E., Hirsch, H. H., 1955. Dispersion-type fuel elements. In: Proceedings of the International Conference on the Peaceful Uses of Atomic Energy, Geneve, Switzerland, August 8-20, 1955.Paper No. P/561.

White, D. W., Beard, A. P., Willis A. H., 1957. Irradiation behavior of dispersion fuels. Knolls Atomic Power Laboratory, Schenectady, New York. United States Atomic Energy Comnission, 1957. KAPL-1909 (available at https://www.osti.gov/servlets/purl/4317012).

Yi-Fu, X., Chen, M., Jing, W., Chen, C., 2010. Manufacturing of U–10 wt% Mo powder by hydride–dehydride processing. Fusion Eng. Des. 85, 1492–1495. https://doi.org/10.1016/j.fusengdes.2010.04.012.